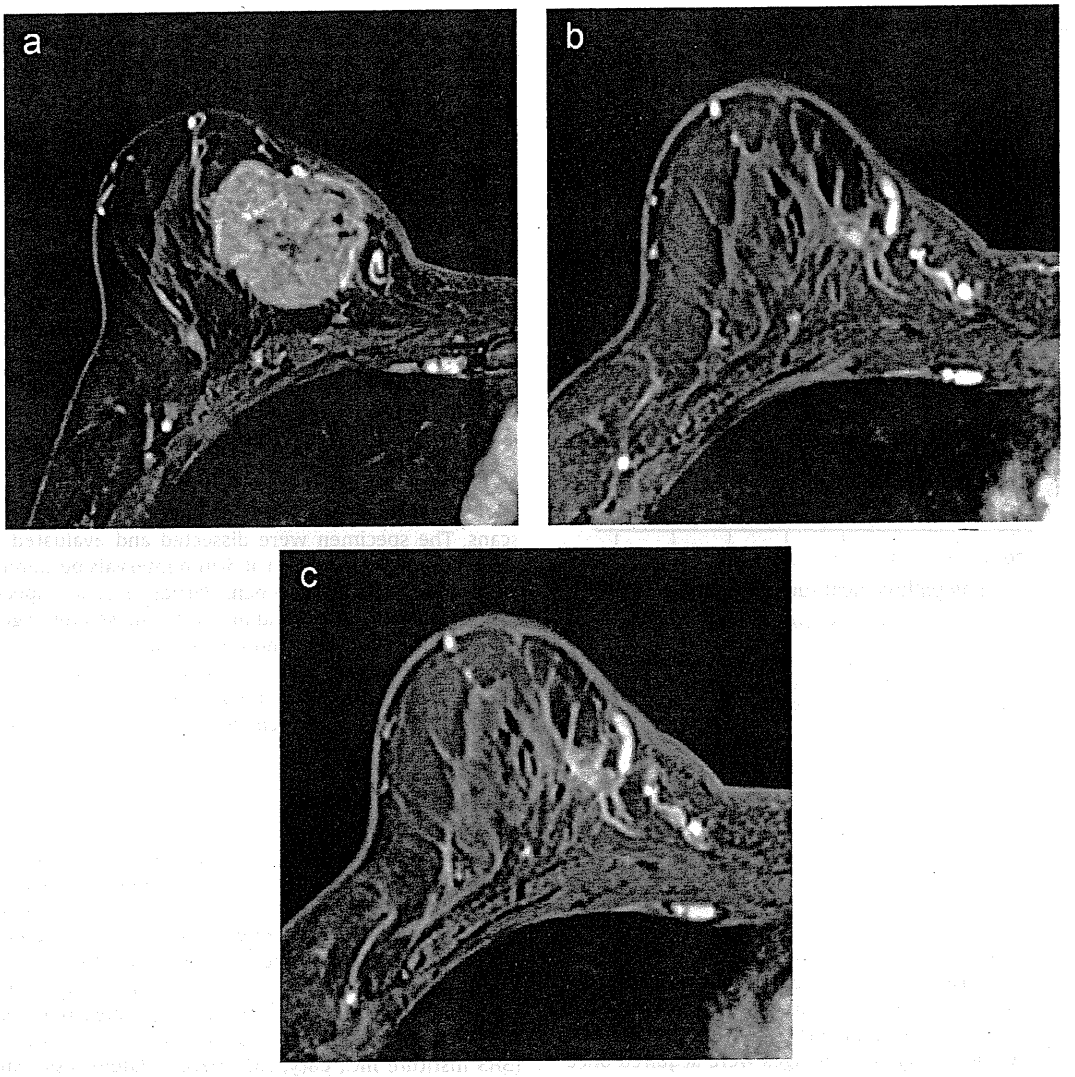

Fig. 3. A concentric shrinkage (CS) case. (A) Dynamic contrast-enhanced T1WI at early phase before NAC. Lobulated mass with rim enhancement was observed at upper-inner area of the right breast. (B) Dynamic contrast-enhanced T1WI at early phase after NAC. The early phase image showed rapid enhanced focus about 4 mm in diameter which was identical to the residual tumor at the pathological specimen. (C) Dynamic contrast-enhanced T1WI at delayed phase after NAC. Delayed image showed heterogeneous non-mass-like enhancement about 23 mm in diameter which was identical to the scar area at the pathological specimen.

CI: 0.66–0.84, $R = 0.92$) and 0.70 (95% CI: 0.56–0.83, $R = 0.90$) for NAC and NAE, respectively (Fig. 1), and no significant interaction was observed between them ($p = 0.46$). In contrast, the analysis of interaction between shrinkage patterns (Fig. 2) revealed regression coefficients of slopes as 1.02 (95% CI: 0.87–1.17, $R = 0.92$) and 0.68 (95% CI: 0.60–0.77, $R = 0.92$), respectively for CS and DS with significant difference ($p < 0.01$). In subgroup analyses by residual tumor size, this result was confirmed when lesion size by MRI was larger than 20 mm (regression coefficients (95% CI): 0.99 (0.47–1.51, $R = 0.91$) and 0.67 (0.51–0.83, $R = 0.94$)), but the difference between CS and DS was not found, when residual tumor size by MRI was equal to or less than 20 mm (1.08 (0.94–1.21, $R = 0.95$) and 1.11 (0.86–1.36, $R = 0.84$)).

4. Discussion

MRI enabled fairly accurate measurement of the largest diameter after NAE as well as NAC, with slight underestimation in both cases, and no significant difference was observed between NAE and NAC in this study (Fig. 1) despite differences in grades, receptor status, Ki-67 index and others between NAE and NAC [10]. Correct visualization of residual tumor after presurgical therapy is highly important, because breast-conserving surgery can be adopted when residual tumor is small. It significantly lessens the burden on patients [16] and is important for prognosis, because overall and disease free survival is higher in cases of pathological CR [3]. Compared to palpation, mammography and ultrasound, MRI is more accurate and reliable for evaluation of residual tumor after NAC [4].

MRI provided good correlation of residual tumor size in general compared with pathological evaluation, however, there was a difference dependent on shrinkage patterns, i.e., CS vs. DS. Tumors showing CS were overestimated (Fig. 2), but only to a very slight degree (Fig. 3). It has been reported that overestimation of residual tumor size by MRI compared with pathology was caused by inclusion of ductal carcinoma in situ (DCIS)[7] and reactive changes [17]. Differential diagnosis of DCIS and invasive ductal carcinoma (IDC) can be challenging with MRI [7]. For pathological TNM staging, DCIS is not considered as a residual lesion, and consequently the overestimation on MRI is considered inevitable.

Please cite this article in press as: Takeda K, et al. MRI evaluation of residual tumor size after neoadjuvant endocrine therapy vs. neoadjuvant chemotherapy. Eur J Radiol (2011), doi:10.1016/j.ejrad.2011.05.013

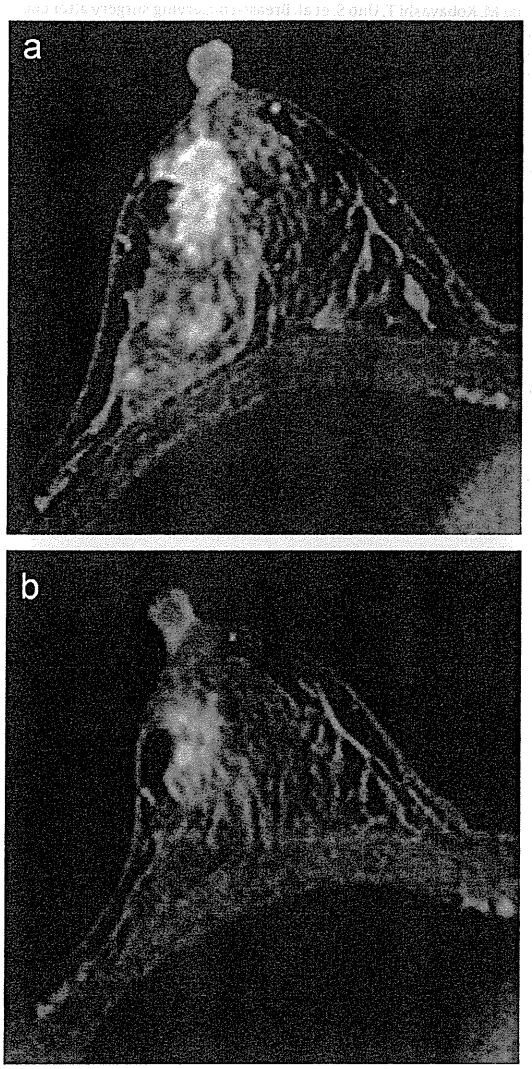

Fig. 4. Underestimation in a dendritic shrinkage (DS) case. (A) Dynamic contrast-enhanced T1WI at early phase before NAE. There were an irregular shaped mass near the nipple and multiple non-mass-like enhancements peripherally. (B) Dynamic contrast-enhanced T1WI at early phase after NAE. The tumor shrank as a whole. However, there remained many small tumor foci scattered at periphery in pathological evaluation. Small lesions were not well detected on MRI.

Underestimation of residual tumor size compared with pathology was observed, when little or no enhancement was present in the residual tumor where tumor cell density was low. Such cases were more frequent in DS cases (Fig. 4) as was previously reported [7,18], and a caution has to be paid for resection. Most of the large-size residual tumors had the DS pattern, and no difference in MR estimation was found between CS and DS when residual tumor size was equal to or less than 2 cm on MRI. It may suggest that residual tumor size could be another factor for underestimation as well as the shrinkage patterns. A tendency for underestimation in the DS cases was reported in a CT study [18]. They named DS pattern as "shrinkage with residual multi-nodular lesions," because "these lesions were characterized histologically by the presence of numerous viable cells with fibrous tissue spread throughout the original tumor bed," which was the case in our histopathological results. Another study called DS pattern as "nest or rim pattern," and found that it had lower agreement in size evaluation between MRI and histopathology [7]. Reduction in enhancement and washout may be caused by disappearance of tumor vessels by systemic therapies [19].

Major factors that affect precision of residual tumor size measurement appear to include differences in breast form and measurement planes between MR images and specimen. The resection specimen is generally soft and may spread flat [7], which were considered inevitable and may hold true for any case in general (R5). Interobserver or intraobserver variation may seem to affect precision of measurement. But interobserver variation in measuring residual tumor size in contrast-enhanced MRI was reported to be 11%, and high accuracy is expected [5]. Accuracy of MRI evaluation would be improved by including other method such as 3D volume MRI data and computer assisted detection system [20].

Some limitations may exist in this study. There were some variations in regimens of NAC and NAE. They were customized for each individual and were another confounding factor. The other issue is the selection bias for NAE patients. They were selected based on the St. Gallen Consensus Guideline 2007 or 2009, and were strongly positive for hormonal receptor, low to intermediate tumor grade and had less than 30% for Ki-67 index. Not all selection of NAE or NAC was conducted in accordance with the guideline, because some patients selected their own therapy otherwise. There also exist some variances in tumor characteristics (see Tables 1 and 2).

In conclusion, whether NAC or NAE was applied, contrast enhanced MRI enables fairly accurate measurement of the largest diameter. However, it tends to underestimate the residual tumor size, especially when the tumor shrank in DS pattern. Caution has to be paid when evaluating residual tumor size with MRI, taking differences not in kinds of therapeutic methods but in shrinkage patterns in mind.

References

[1] Tardivon A, Ollivier L, El Khoury C, Thibault F. Monitoring therapeutic efficacy in breast carcinomas. Eur Radiol 2006;16(11):2549–58.
[2] van der Hage JA, van de Velde CJ, Julien JP, Tubiana-Hulin M, Vandervelden C, Duchateau L. Preoperative chemotherapy in primary operable breast cancer: results from the European Organization for Research and Treatment of Cancer trial 10902. J Clin Oncol 2001;19(22):4224–37.
[3] Wolmark N, Wang J, Mamounas E, Bryant J, Fisher B. Preoperative chemotherapy in patients with operable breast cancer: nine-year results from National Surgical Adjuvant Breast and Bowel Project B-18. J Natl Cancer Inst Monogr 2001;30:96–102.
[4] Balu-Maestro C, Chapellier C, Bleuse A, Chanalet I, Chauvel C, Largillier R. Imaging in evaluation of response to neoadjuvant breast cancer treatment benefits of MRI. Breast Cancer Res Treat 2002;72(2):145–52.
[5] Partridge S, Gibbs J, Lu Y, Esserman L, Sudilovsky D, Hylton N. Accuracy of MR imaging for revealing residual breast cancer in patients who have undergone neoadjuvant chemotherapy. Am J Roentgenol 2002;179(5):1193–9.
[6] Rosen E, Blackwell K, Baker J, et al. Accuracy of MRI in the detection of residual breast cancer after neoadjuvant chemotherapy. Am J Roentgenol 2003;181(5):1275–82.
[7] Kim HJ, Im YH, Han BK, et al. Accuracy of MRI for estimating residual tumor size after neoadjuvant chemotherapy in locally advanced breast cancer: relation to response patterns on MRI. Acta Oncol 2007;46(7):996–1003.
[8] Connolly R, Stearns V. A multidisciplinary approach to neoadjuvant therapy for primary operable breast cancer. Challenges and opportunities. Oncology (Williston Park) 2010;24(2):135–43.
[9] Sachelarie I, Grossbard ML, Chadha M, Feldman S, Ghesani M, Blum RH. Primary systemic therapy of breast cancer. Oncologist 2006;11(6):574–89.
[10] Goldhirsch A, Ingle J, Gelber R, et al. Thresholds for therapies: highlights of the St. Gallen International Expert Consensus on the primary therapy of early breast cancer 2009. Ann Oncol 2009;20(8):1319–29.
[11] Thibault F, Nos C, Meunier M, et al. MRI for surgical planning in patients with breast cancer who undergo preoperative chemotherapy. Am J Roentgenol 2004;183(4):1159–68.
[12] Nakamura S, Kenjo H, Nishio T, Kazama T, Doi O, Suzuki K. Efficacy of 3D-MR mammography for breast conserving surgery after neoadjuvant chemotherapy. Breast Cancer 2002;9(1):15–9.
[13] Chen JH, Feig B, Agrawal G, et al. MRI evaluation of pathologically complete response and residual tumors in breast cancer after neoadjuvant chemotherapy. Cancer 2008;112(1):17–26.

Please cite this article in press as: Takeda K, et al. MRI evaluation of residual tumor size after neoadjuvant endocrine therapy vs. neoadjuvant chemotherapy. Eur J Radiol (2011), doi:10.1016/j.ejrad.2011.05.013

[14] Goldhirsch A, Wood W, Gelber R, et al. Progress and promise: highlights of the international expert consensus on the primary therapy of early breast cancer 2007. Ann Oncol 2007;18(7):1133–44.
[15] Rinck PA, Muller RN. Field strength and dose dependence of contrast enhancement by gadolinium-based MR contrast agents. Eur Radiol 1999;9(5):998–1004.
[16] Deo SV, Bhutani M, Shukla NK, Raina V, Rath GK, Purkayasth J. Randomized trial comparing neo-adjuvant versus adjuvant chemotherapy in operable locally advanced breast cancer (T4b N0-2 M0). J Surg Oncol 2003;84(4):192–7.
[17] Liberman L, Morris E, Lee M, et al. Breast lesions detected on MR imaging: features and positive predictive value. Am J Roentgenol 2002;179(1):171–8.
[18] Tozaki M, Kobayashi T, Uno S, et al. Breast-conserving surgery after chemotherapy: value of MDCT for determining tumor distribution and shrinkage pattern. Am J Roentgenol 2006;186(2):431–9.
[19] Wasser K, Sinn H, Fink C, et al. Accuracy of tumor size measurement in breast cancer using MRI is influenced by histological regression induced by neoadjuvant chemotherapy. Eur Radiol 2003;13(6):1213–23.
[20] Partridge SC, Gibbs JE, Lu Y, et al. MRI measurements of breast tumor volume predict response to neoadjuvant chemotherapy and recurrence-free survival. Am J Roentgenol 2005;184(6):1774–81.

Please cite this article in press as: Takeda K, et al. MRI evaluation of residual tumor size after neoadjuvant endocrine therapy vs. neoadjuvant chemotherapy. Eur J Radiol (2011), doi:10.1016/j.ejrad.2011.05.013

Apparent Diffusion Coefficient as an MR Imaging Biomarker of Low-Risk Ductal Carcinoma in Situ: A Pilot Study[1]

Mami Iima, MD
Denis Le Bihan, MD, PhD
Ryosuke Okumura, MD, PhD
Tomohisa Okada, MD, PhD
Koji Fujimoto, MD, PhD
Shotaro Kanao, MD
Shiro Tanaka, PhD
Masakazu Fujimoto, MD
Hiromi Sakashita, MD, PhD
Kaori Togashi, MD, PhD

Purpose: To evaluate the potential of apparent diffusion coefficients (ADCs) obtained at quantitative diffusion-weighted magnetic resonance (MR) imaging of the breast as a biomarker of low-grade ductal carcinoma in situ (DCIS).

Materials and Methods: This retrospective study was approved by an institutional review board, and the requirement to obtain informed consent was waived. Twenty-two women (age range, 36–75 years; mean age, 56.4 years) with pure DCIS (seven with low-grade DCIS, five with intermediate-grade DCIS, and seven with high-grade DCIS) and three with microinvasion underwent breast MR imaging at 1.5 T between January 2008 and November 2010. MR examinations included contrast material–enhanced (gadoteridol) T1-weighted imaging and diffusion-weighted MR imaging with b values of 0 and 1000 sec/mm^2. ADC maps were generated. The distributions of the ADCs in regions of interest covering the lesions were compared among the three grades by using linear mixed-model analysis, and the discriminatory power of the lesion minimum ADC was determined with receiver operating characteristic analysis.

Results: The mean ADC was 1.42×10^{-3} mm^2/sec (95% confidence interval [CI]: 1.31×10^{-3} mm^2/sec, 1.54×10^{-3} mm^2/sec) for low-grade DCIS, 1.23×10^{-3} mm^2/sec (95% CI: 1.10×10^{-3} mm^2/sec, 1.36×10^{-3} mm^2/sec) for intermediate-grade DCIS, 1.19×10^{-3} mm^2/sec (95% CI: 1.08×10^{-3} mm^2/sec, 1.30×10^{-3} mm^2/sec) for high-grade DCIS, and 2.06×10^{-3} mm^2/sec (95% CI: 1.94×10^{-3} mm^2/sec, 2.18×10^{-3} mm^2/sec) for normal breast tissue. The mean ADCs for high- and intermediate-grade DCIS were significantly lower than that for low-grade DCIS ($P < .01$ and $P = .03$, respectively), and the mean ADC for low-grade DCIS was significantly lower than that for normal tissue ($P < .001$). The lesion minimum ADC for low-grade DCIS was also significantly higher than that for high- and intermediate-grade DCIS ($P < .01$). A threshold of 1.30×10^{-3} mm^2/sec for the minimum ADC in the diagnosis of low-grade DCIS had a specificity of 100% (12 of 12 patients; 95% CI: 73.5%, 100%) and a positive predictive value of 100% (four of four patients; 95% CI: 39.8%, 100%).

Conclusion: These preliminary results suggest that quantitative diffusion-weighted MR imaging could be used to identify patients with low-grade DCIS with very high specificity. If the results of this study are confirmed, this approach could potentially spare those patients from invasive approaches such as mastectomy or axillary lymph node excision.

[1] From the Department of Diagnostic Imaging and Nuclear Medicine (M.I., T.O., K.F., S.K., K.T.) and Human Brain Research Center (D.L.B.), Kyoto University Graduate School of Medicine, 54 Shogoin Kawaharacho, Sakyoku, Kyoto 606-8507, Japan; Departments of Radiology (M.I., R.O.) and Pathology (M.F., H.S.), Kitano Hospital, Osaka, Japan; Neurospin, CEA-Saclay, Gif-sur-Yvette, France (D.L.B.); and Translational Research Center, Kyoto University Hospital, Kyoto, Japan (S.T.). Received October 7, 2010; revision requested November 22; revision received February 1, 2011; accepted March 16; final version accepted April 20. **Address correspondence to** M.I. (e-mail: *mamiiima@kuhp.kyoto-u.ac.jp*).

With the advent of widespread mammographic screening for breast cancer in the early to mid-1980s, the detection of ductal carcinoma in situ (DCIS) has increased worldwide. Currently, DCIS accounts for 20%–30% of all newly diagnosed breast cancers in the United States and approximately 20% of cases detected with mammography (1). An important issue, however, is that one cannot predict whether DCIS will evolve to invasive ductal carcinoma. Hence, even though low-grade DCIS may be considered a nonlethal type of tumor, all cases of DCIS are usually treated as though they will become invasive ductal carcinoma. Indeed, recent studies have pointed out that the natural history of low-grade DCIS can extend more than 4 decades and that it is unlikely to become invasive (2,3).

Recent immunohistochemical studies have revealed that, unlike adenoma-carcinoma of the colon, which evolves following a single line, benign proliferative breast disease, some low-grade DCIS, most high-grade DCIS, and invasive carcinoma develop through distinct pathways (4). Those findings suggest that different therapeutic approaches could be proposed according to DCIS grade. Hence, there is a need for more accurate DCIS grading at the time of the initial diagnosis to customize the therapeutic approach. With mammography, it is possible to suspect the presence of high-grade lesions on the basis of the morphologic characteristics of microcalcifications (5); however, grading of DCIS remains difficult, with sparse biopsy sampling, because high- and low-grade components may coexist in a patient or even within one duct.

Lately, breast magnetic resonance (MR) imaging has been successfully introduced in the management of breast cancer—particularly DCIS (6). Although mammography can depict 80%–85% of all DCIS, the sensitivity of MR imaging in the accurate assessment of the extent of DCIS reaches 89%, which is much higher than that of either mammography or ultrasonography (US) (55% and 47%, respectively) (7). There is increasing evidence to suggest that, overall, breast MR imaging may be more sensitive than mammography—especially in the diagnosis of high-grade DCIS (8,9).

More recently, diffusion-weighted MR imaging has been introduced for cancer imaging. Diffusion-weighted imaging is highly sensitive to tissue microstructure (10,11), and it has been observed that the apparent diffusion coefficient (ADC) is significantly reduced in primary or secondary cancer tissues (12–14)—although the exact mechanism between diffusion reduction and cell proliferation remains unclear (15). Diffusion-weighted imaging was found to have a very high sensitivity of 97% in the detection of breast malignancy (16). Diffusion-weighted images and quantitative ADC maps have been successfully used to differentiate between benign and malignant breast lesions as well as to depict tumor extension (17–19) and may have the potential to depict many mammographically and clinically occult breast carcinomas (20). In light of those encouraging results, we performed this study to evaluate the potential of ADCs obtained at quantitative diffusion-weighted MR imaging of the breast as a biomarker of low-grade DCIS.

Advances in Knowledge

- The apparent diffusion coefficients (ADCs) of high- and intermediate-grade ductal carcinoma in situ (DCIS) lesions were significantly lower than those of low-grade DCIS ($P < .01$, $P = .03$, respectively), and there was a significant negative trend between mean ADC and tumor grade ($P < .01$).
- With use of receiver operating characteristic analysis, a cutoff value for the lesion minimum ADC was established under the restriction of 100% specificity (95% confidence interval: 73.5%, 100%) while maximizing sensitivity; all four patients whose minimum ADCs were above a threshold of 1.30×10^{-3} mm^2/sec had low-grade DCIS.

Implication for Patient Care

- Our preliminary results suggest that quantitative diffusion-weighted MR imaging could be used to identify patients with low-grade, low-risk DCIS with very high specificity and, if the results are confirmed, has the potential to spare patients from invasive approaches (eg, mastectomy or axillary lymph node excision); in addition, this approach could potentially decrease the anxiety of women diagnosed with low-risk DCIS by reassuring them of the noninvasive nature of the lesions.

Materials and Methods

Patients

Institutional review board approval was obtained, and the requirement to obtain informed consent was waived owing to the retrospective nature of this study. This study was a retrospective review of images from 25 women in whom DCIS was diagnosed after biopsy at Kitano Hospital between January 2008 and November 2010. DCIS was first suspected after patients underwent physical examination, mammography, and US. MR

Published online before print
10.1148/radiol.11101892 **Content codes:** BR OI BQ

Radiology 2011; 260:364–372

Abbreviations:
ADC = apparent diffusion coefficient
CI = confidence interval
DCIS = ductal carcinoma in situ
ROC = receiver operating characteristic
ROI = region of interest

Author contributions:
Guarantors of integrity of entire study, M.I., D.L.B., K.T.; study concepts/study design or data acquisition or data analysis/interpretation, all authors; manuscript drafting or manuscript revision for important intellectual content, all authors; approval of final version of submitted manuscript, all authors; literature research, M.I., D.L.B., R.O., T.O., S.T., K.T.; clinical studies, M.I., R.O., S.K., S.T., M.F., H.S., K.T.; experimental studies, D.L.B., K.T.; statistical analysis, D.L.B., K.F., K.T.; and manuscript editing, M.I., D.L.B., T.O., K.F., S.K., K.T.

Potential conflicts of interest are listed at the end of this article.

imaging was performed before or 2 weeks after biopsy to avoid artifacts. Mammography showed microcalcifications in 17 of the 25 patients and focal asymmetry suspicious for malignancy in five. There were no suspicious findings at mammography in three patients; however, two of the three patients were suspected of having DCIS at breast US and one patient had nipple erosion. Only patients with pure DCIS (without microinvasion or invasive breast cancer elsewhere) were enrolled in this study. Three patients were excluded from the study. Two patients (one with intermediate DCIS and one with low-to-intermediate-grade DCIS) were excluded because their diffusion-weighted images showed no contrast with the background owing to a very low signal-to-noise ratio, and one patient (with intermediate DCIS) was excluded because of incomplete fat suppression. Hence, 22 patients (age range: 36–75 years; mean age, 56.4 years) were initially included in this study. Seven patients had low-grade DCIS, five had intermediate-grade DCIS, seven had high-grade DCIS, and three had DCIS with microinvasion. One patient had a low-to-intermediate-grade DCIS, which was considered low-grade DCIS because the lesion was classified as Van Nuys Prognostic Index 4, which is associated with the best DCIS prognosis (21,22). Because the status of DCIS lesions with microinvasion is still controversial (23), the three patients with microinvasion were excluded from the statistical analysis performed only with pure DCIS cases.

MR Image Acquisition

Breast MR imaging was performed by using a 1.5-T unit (Intera and Achieva; Philips Healthcare, Eindhoven, the Netherlands) equipped with a dedicated four-channel breast array coil. The following images were acquired after obtaining localizer images: bilateral sagittal fat-suppressed T2-weighted images (4937/90 [repetition time msec/echo time msec], 20-cm field of view, 256 × 256 matrix, 4-mm-thick sections, 162-second acquisition time); fat-suppressed, diffusion-weighted echo-planar images (8000/96; 40-cm field of view; 128 × 104 matrix interpolated to 256 × 256 [ie, 1.56 × 1.56-mm resolution]; parallel acquisition factor of 2; 5-mm-thick sections; 182-second acquisition time; and application of motion probing gradient pulses along the x, y, and z directions with b values of 0 and 1000 sec/mm^2); and free-breathing dynamic contrast material–enhanced MR images, which were obtained by using a three-dimensional fat-suppressed T1-weighted gradient-echo sequence (6.1/3.5, 15° flip angle, 40-cm field of view, 400 × 400 matrix, 2-mm-thick sections reconstructed to 0.78 × 0.78 × 1-mm resolution, 255-second acquisition time), which were acquired before and immediately after infusion of 0.2 mL/kg gadoteridol (ProHance; Bracco-Eisai, Tokyo, Japan). Central k-space data were acquired first to catch early contrast enhancement. T1-weighted images were also acquired 9 minutes after infusion, but those images were not considered in this study. With diffusion-weighted imaging data, the quantitative diffusion (ADC) was calculated on a voxel-by-voxel basis as follows: ADC = $(1/b) \times \ln (S_0/S)$, where S_0 and S are the signal intensities of each voxel obtained with values of 0 and 1000 sec/mm^2, respectively.

Data Postprocessing

Two independent readers (M.I. [radiologist A] and R.O. [radiologist B], with 3 and 6 years of experience in breast MR imaging, respectively) manually drew regions of interest (ROIs) on the diffusion-weighted images (b = 1000 sec/mm^2) (Figs 1, 2). The readers were blinded to the final pathologic results. ROIs were placed in regions with high signal intensity on the diffusion-weighted images; the contrast and morphologic characteristics at the early phase of contrast-enhanced T1-weighted imaging and T2-weighted imaging were used to guide ROI placement to avoid areas of T2 shine-through that are usually found in necrotic or cystic parts. The signal intensity of the lesion on the diffusion-weighted images was visually classified as high or low compared with that of the corresponding background breast tissue. T1-weighted images were also used retrospectively to assess the nature of borderline lesions with very high or very low ADCs. ROIs were defined as slightly smaller than the actual lesions to reduce partial volume effects, but only ROIs larger than 20 mm^2 were considered as meaningful and retained for further analysis. Because DCIS is usually a multifocal disease, several ROIs were drawn to depict each lesion. Hence, the number of ROIs for each patient varied from one to eight (Fig 3). Control ROIs were drawn in the normal homogeneous breast parenchyma in the center of the contralateral breast, avoiding contamination by fatty tissue. The average of mean ROI sizes of normal tissues was 140.1 mm^2 (range, 106.8–175.0 mm^2). The ROIs were then copied and pasted onto the corresponding ADC map for quantitative analysis. For each ROI, we extracted the mean ADC and the ROI area. The total lesion size, which was defined as the sum of the areas of all ROIs used to depict the lesion for each patient, was also compared among each grade. Because the scope of this study was purely focused on quantitative diffusion-weighted MR imaging, the kinetics of contrast enhancement were not considered. The value of contrast-enhanced MR imaging for DCIS has been reported elsewhere (8,24).

Histopathologic Analysis

Histopathologic analysis was performed with use of specimens obtained from surgery (mastectomy or lumpectomy). Blocks were processed, and sections were cut and stained with hematoxylin and eosin according to standard pathology protocols and studied by experienced pathologists (H.S. and M.F., with 10 and 5 years of experience in breast pathology, respectively). Histologic circumscription without irregular, infiltrative, or fingerlike extensions into the adjacent stroma was regarded as indicative of a noninvasive growth pattern. Nuclear grade and presence of necrosis were assessed and the DCIS grade was established (25). On slides where microinvasion was suspected, immunohistochemistry was performed by using an automated immunostainer (Ventana BenchMark AutoStainer; Ventana Medical

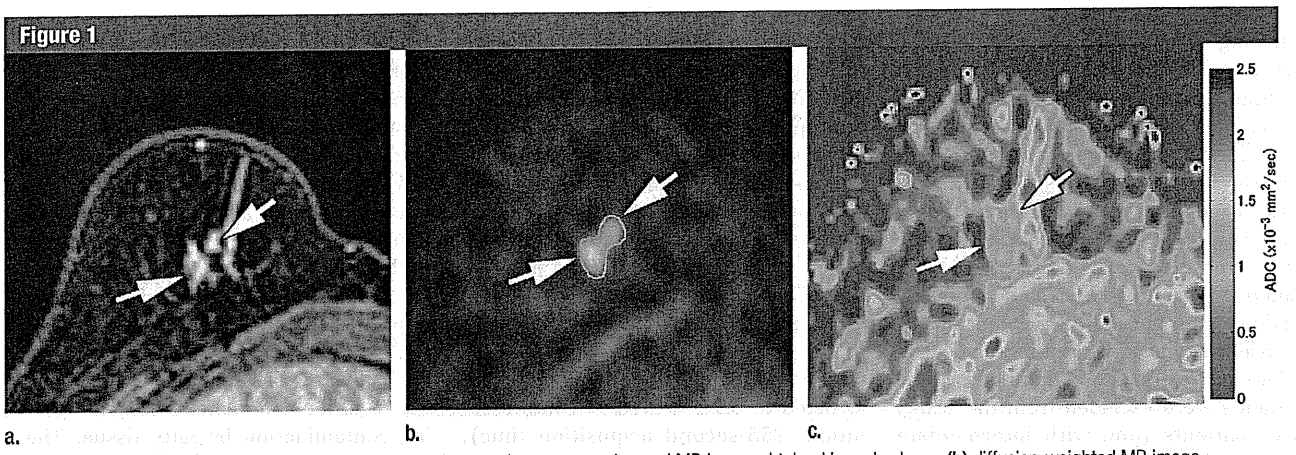

Figure 1: High-grade DCIS in a 56-year-old woman. **(a)** Dynamic contrast-enhanced MR image obtained in early phase, **(b)** diffusion-weighted MR image ($b = 1000$ sec/mm^2), and **(c)** ADC map. **(a)** Areas of homogeneous nonmasslike enhancement (arrows) are shown; this image was used to identify lesions and define corresponding ROIs on **b** (arrows), where lesions are visible as areas of high signal intensity. **(c)** Lesion exhibits areas with light blue contours (arrows), which are indicative of low ADC.

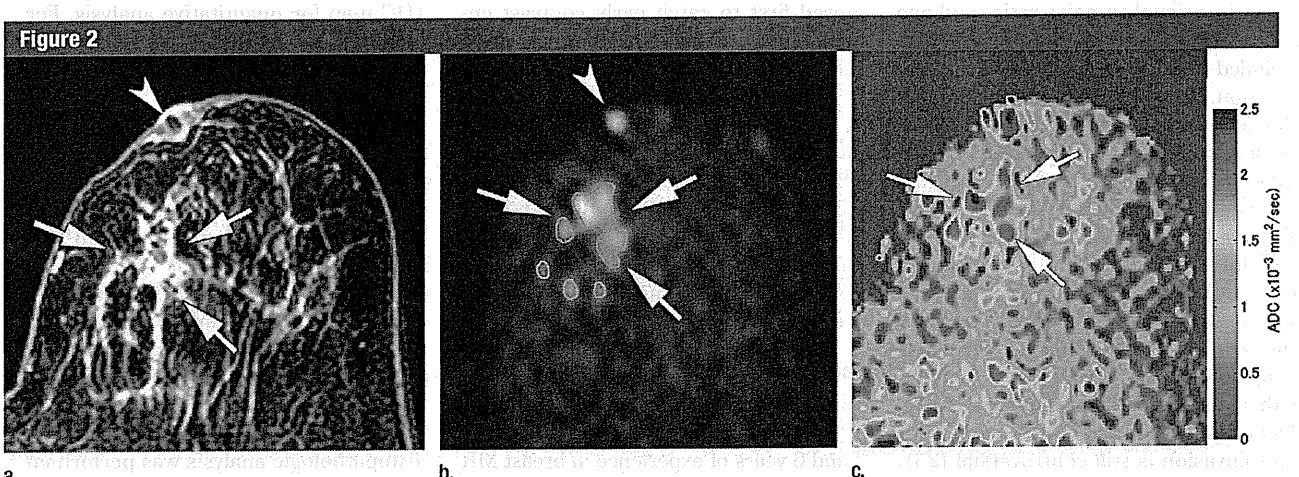

Figure 2: Low-grade DCIS (arrows) in a 68-year-old woman. **(a)** Dynamic contrast-enhanced MR image obtained in early phase, **(b)** diffusion-weighted MR image ($b = 1000$ sec/mm^2), and **(c)** ADC map. In **c**, lesion has orange-red contours (corresponding to high ADC). In **b**, only ROIs outlined in green were analyzed; blue ROIs were excluded because they were smaller than 20 mm^2. The area of high signal intensity (arrowhead) on **b** was not outlined because it did not enhance on contrast-enhanced image (arrowhead). This area turned out to be nipple discharge.

Systems, Tucson, Ariz) with antibodies against two myoepithelial markers, CD10 (diluted 1:50; 56C6, Novocastra, Newcastle, United Kingdom) and p63 (diluted 1:25; 7JUL, Novocastra). Immunoreactivity for CD10 and p63 was evaluated at the periphery of each circumscribed nest, and lesions lacking immunoreactivity for myoepithelial markers were diagnosed as microinvasion.

Statistical Analysis

To assess the reliability of our multiple ROI approach, the interobserver variability between radiologists A and B was evaluated by using intraclass correlation coefficient type "2,1" and the Pearson correlation coefficient for the mean ADC in the ROI and ROI size. The level of correlation was defined as very strong if $r = 1.0$–0.9, strong if $r = 0.9$–0.7, moderate if $r = 0.7$–0.5, and weak if $r = <0.5$. Then, ROIs from both radiologists were merged, taking the average value for the mean ADC and ROI size analyses.

To evaluate whether distributions of ADCs and ROI sizes differed among the three grades, "ROI-based" analysis was performed by using the mean ADC and the ROI sizes of all ROIs. We used linear mixed-model analysis for repeated measurement data (26) and estimated the least-square means (adjusted means) and the 95% confidence intervals (CIs) of the ADCs and ROI sizes in each grade adjusted for within-patient correlation. The P values for the differences between low-grade DCIS and intermediate- or high-grade DCIS were adjusted for multiple comparisons with use of the Hochberg procedure. A P value from a

Figure 3

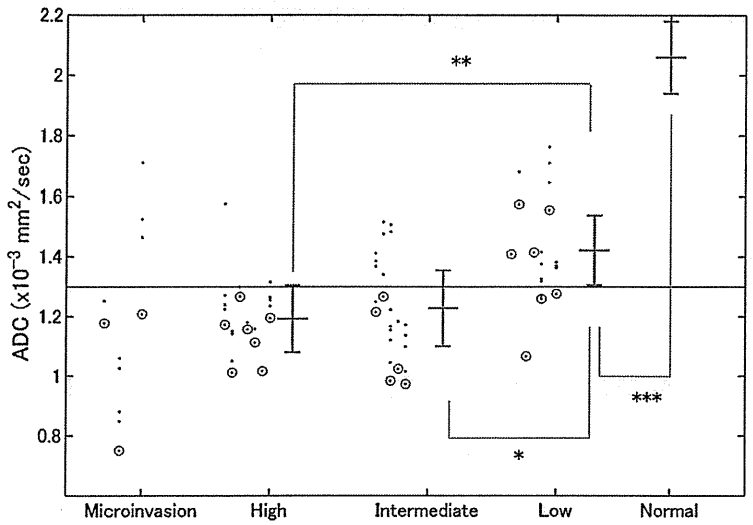

Figure 3: Graph shows distribution of ADCs for all ROIs. The mean ADC for each ROI (all 22 patients) is plotted, with data from each patient given in vertical columns. The number of ROIs per patient varied from one to eight. Patients are grouped according to lesion grade. Red circles = minimum ADC for each patient. The adjusted mean ADC and its 95% CI are shown for each grade as a vertical line to the right of each grade. The vertical line on right side of graph = mean ADC and 95% CI for normal breast tissue. The red line = ADC threshold of 1.30×10^{-3} mm²/sec for diagnosis of low-grade DCIS. All four patients whose minimum ADC was above this line had low-grade DCIS. * = $P < .05$ for comparison of intermediate- and low-grade DCIS, ** = $P < .01$ for comparison of high- and low-grade DCIS, and *** = $P < .001$ for comparison of low-grade DCIS and normal tissue. (ADC values for the three patients with microinvasion are shown for completeness, although they were excluded from statistical analysis.)

trend test was also calculated by using linear mixed models. The sample mean ADC of the low-grade DCIS lesions was compared with that of the normal breast tissue with a paired t test. Total lesion sizes for all patients across low, intermediate, and high grades were compared by using linear model analysis by estimating their sample means and their 95% CIs in each grade.

After establishing a statistically significant (negative) correlation between tumor grade and ADC, we tried to define a "patient-based" diagnostic procedure to identify low-grade lesions with the highest specificity. We hypothesized that the potentially most active part of the lesion is associated with the lowest ADC, and we investigated the diagnostic value of the lesion minimum ADC (defined as the ADC of the ROI with the lowest ADC within the lesion) for each patient. The minimum ADCs across low, intermediate, and high grades were first compared by estimating the sample means and the 95% CIs in each grade. P values for the differences between low-grade DCIS and intermediate- or high-grade DCIS were adjusted for multiple comparisons by using the Hochberg procedure. A P value from a trend test was also calculated by using general linear models.

The effectiveness of this diagnostic procedure in the differentiation of low-grade DCIS from non-low-grade DCIS was evaluated by using receiver operating characteristic (ROC) analysis. With use of ROC analysis, a cutoff value for the lesion minimum ADC was established under the restriction of 100% specificity while maximizing sensitivity.

For the ROI and lesion size statistical analysis, a log transformation was used to account for the skewness of the distribution. For all tests, $P < .05$ was considered indicative of a statistically significant difference. All statistical analyses was conducted by using software (Medcalc, version 11.3.2.0 [MedCalc Software, Mariakerke, Belgium], and SAS, version 9.2 [SAS Institute, Cary, NC]).

Results

MR Imaging Findings

The typical appearance of high- and low-grade tumors on contrast-enhanced T1-weighted images, diffusion-weighted images (b = 1000 sec/mm²), and ADC maps is shown in Figures 1 and 2. Two cases of low-grade DCIS exhibited low contrast, whereas all other lesions showed high contrast with surrounding tissue on diffusion-weighted images (b = 1000 sec/mm²). Results from all patients are summarized in Figure 3.

Some low-grade DCIS lesions contained parts with very low ADCs—even lower than those of high-grade DCIS. In one patient, the minimum ADC was 1.07×10^{-3} mm²/sec; this was probably related to bleeding or high protein content, as suspected from very high signal intensities on the T1-weighted images. Another patient with a high-grade lesion had one region with a very high ADC (1.58×10^{-3} mm²/sec). The lesion was situated very near the nipple, and a collection of mucous or liquid due to the obstruction of the duct by the lesion may have resulted in the high ADC.

Interobserver Variability

Radiologist A identified 69 ROIs (24 for high-grade DCIS, 24 for intermediate-grade DCIS, and 21 for low-grade DCIS), and radiologist B identified 66 ROIs (22 for high-grade DCIS, 24 for intermediate-grade DCIS, and 20 for low-grade DCIS). The Pearson correlation of the 66 ROIs was strong (0.91 for mean ADC, 0.95 for ROI size), and the intraclass correlation of the 66 ROIs was moderate (0.72 for mean ADC, 0.56 for ROI size). It is important to note that the lesion minimum ADC (see below) was not found in the three ROIs identified by radiologist A and not by radiologist B.

Comparison of ADCs across Grades

The adjusted mean ADC of all ROIs was 1.42×10^{-3} mm²/sec (95% CI: 1.31×10^{-3} mm²/sec, 1.54×10^{-3} mm²/sec) for low-grade DCIS, 1.23×10^{-3} mm²/sec (95% CI: 1.10×10^{-3} mm²/sec, 1.36×10^{-3} mm²/sec) for intermediate-grade DCIS, and 1.19×10^{-3} mm²/sec (95% CI: 1.08×10^{-3} mm²/sec, 1.30×10^{-3} mm²/sec) for high-grade DCIS (Table 1). The mean ADC of high-grade DCIS lesions was significantly lower than that of low-grade DCIS lesions ($P < .01$). The mean ADC of intermediate-grade DCIS was also significantly lower than that of low-grade DCIS ($P = .03$), and there was a significant negative trend between mean ADC and lesion grade ($P < .01$) despite the overlap between ADCs. The sample mean in normal tissue was 2.06×10^{-3} mm²/sec (range, $1.32–2.47 \times 10^{-3}$ mm²/sec; 95% CI: 1.94×10^{-3} mm²/sec, 2.18×10^{-3} mm²/sec). The mean ADC of low-grade DCIS was significantly lower than that of normal breast tissues ($P < .001$).

The mean minimum ADC was 1.35×10^{-3} mm²/sec (95% CI: 1.24×10^{-3} mm²/sec, 1.46×10^{-3} mm²/sec) for low-grade DCIS, 1.09×10^{-3} mm²/sec (95% CI: 0.97×10^{-3} mm²/sec, 1.22×10^{-3} mm²/sec) for intermediate-grade DCIS, and 1.11×10^{-3} mm²/sec (95% CI: 1.01×10^{-3} mm²/sec, 1.22×10^{-3} mm²/sec) for high grade DCIS (Table 2). The minimum ADC of low-grade DCIS was significantly higher than that of high-grade DCIS ($P < .01$). The minimum ADC of intermediate-grade DCIS was significantly different from that of low-grade DCIS ($P < .01$). There was a significant negative trend between minimum ADC and lesion grade ($P < .01$). The minimum ADCs for the three lesions with microinvasion were 0.75, 1.18, and 1.21×10^{-3} mm²/sec.

Table 1

ROI-Level Comparison of Mean ADCs across Pathologic Grades

Grade	ADC ($\times 10^{-3}$ mm²/sec) Adjusted Mean	Median	Range	95% CI	*P* Value*
Low	1.42	1.41	1.07–1.76	1.31, 1.54	Ref
Intermediate	1.23	1.12	0.97–1.52	1.10, 1.36	.03
High	1.19	1.23	1.01–1.58	1.08, 1.30	<.01

Note.—Results of a trend test showed a significant negative trend between mean ADC and lesion grade ($P < .01$, linear mixed model) despite the overlap between ADCs.

* *P* values reflect the difference in mean ADC from low-grade DCIS. All *P* values were significant after adjustment for multiplicity with the Hochberg procedure. Ref = reference.

Table 2

Patient-Level Comparison of Minimum ADCs across Pathologic Grades

Grade	ADC ($\times 10^{-3}$ mm²/sec) Sample Mean	Range	95% CI	*P* Value*
Low	1.35	1.07–1.55	1.24, 1.46	Ref
Intermediate	1.09	0.98–1.26	0.97, 1.22	<.01
High	1.11	1.00–1.26	1.01, 1.22	<.01

Note.—Results of a trend test showed a significant negative trend between mean ADC and lesion grade ($P < .01$, linear mixed model) despite the overlap between ADCs.

* *P* values reflect the difference in mean ADC from low-grade DCIS. All *P* values were significant after adjustment for multiplicity with the Hochberg procedure. Ref = reference.

Comparison of ROI and Lesion Sizes across Grades

The adjusted means of the ROI sizes were 65.2 mm² (95% CI: 42.8 mm², 99.1 mm²), 88.1 mm² (95% CI: 56.4 mm², 138.7 mm²), and 45.2 mm² (95% CI: 30.2 mm², 67.6 mm²) for low-, intermediate-, and high-grade DCIS, respectively (Table 3). The difference in ROI size between high- and low-grade lesions was not significant ($P = .21$), and there was not a significant negative trend between ROI size and tumor grade ($P = .25$). The sample means of the total lesion sizes were 303.6 mm² (95% CI: 91.4 mm², 515.7 mm²), 521.0 mm² (95% CI: 270.0 mm², 772.0 mm²), and 165.7 mm² (95% CI: 46.4 mm², 377.9 mm²) for low-, intermediate-, and high-grade DCIS, respectively. There was also no statistically significant difference in the total lesion size among grades ($P = .39$). It should be noted that, although the total lesion size reflects the real lesion size, it is actually slightly smaller because only ROIs with a surface larger than 20 mm² were considered.

ROC Curve Analysis

The discriminatory power of the lesion minimum ADC (to differentiate low-grade DCIS from non-low-grade DCIS) was good, with an area under the ROC curve of 0.89 (95% CI: 0.66, 0.99) for radiologist A and 0.88 (95% CI: 0.65, 0.98) for radiologist B (Fig 4).

The minimum ADC to obtain 100% specificity (12 of 12 patients; 95% CI: 73.5%, 100%) while maximizing sensitivity was 1.30×10^{-3} mm²/sec. All four patients whose minimum ADC was above this threshold had low-grade DCIS. On the basis of this threshold, the same four of 19 patients (21%) would have been correctly identified by each of the two radiologists as having low-grade DCIS with a positive predictive value of 100% (four of four patients; 95% CI: 39.8%, 100%) and a specificity of 100% (12 of 12 patients; 95% CI: 73.5%, 100%). None of the patients with intermediate- or high-grade DCIS or microinvasion had a minimum ADC below the threshold. The sensitivity was 57% (four of seven patients; 95% CI: 18.4%, 90.1%), and the negative predictive value was 80% (12 of 15 patients; 95% CI: 51.9%, 95.7%).

Discussion

The diagnosis of DCIS is rapidly increasing because of the widespread use of

Table 3

ROI-Level Comparison of Mean ROI Sizes according to Pathologic Grade

	ROI Size (mm^2)				
Grade	Adjusted Mean*	Median	Range	95% CI	*P* Value†
Low	65.2	63.5	24.5–272.0	42.8, 99.1	Ref
Intermediate	88.1	96.3	35.5–334.5	56.4, 138.7	.32
High	45.2	42.5	24.5–144.5	30.2, 67.6	.21

Note.—Results of a trend test did not show a significant negative trend between ROI size and tumor grade ($P = .25$, linear mixed model).

* A log transformation was used to account for the skewness of the distribution on the histogram. Adjusted means were converted back with an inverse transformation.

† *P* values reflect the difference in mean ROI size from low-grade DCIS. Ref = reference.

Figure 4

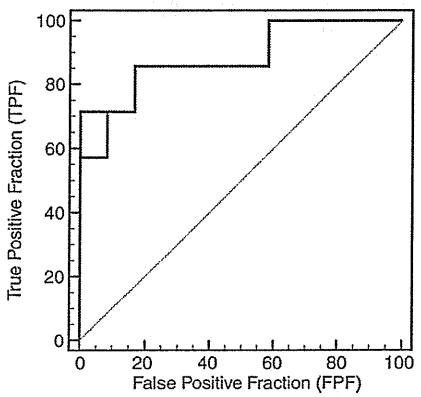

Figure 4: Graph shows ROC curves for differentiating low-grade DCIS from other grades of DCIS on the basis of minimum ADC values. Red line = radiologist A, blue line = radiologist B. The area under the ROC curve was 0.89 (95% CI: 0.66, 0.99) for radiologist A and 0.88 (95% CI: 0.65, 0.98) for radiologist B. Diagonal reference line indicates worst discriminatory power.

screening mammography. Even though DCIS lesions usually do not become invasive, patients in whom DCIS is diagnosed are usually treated as though they will have invasive carcinoma. The social, ethical, and economic consequences of such management are huge: More than 40% of women with DCIS undergo mastectomy, at a rate of some 10000 per year (1). Clearly one should look for new biomarkers to better predict the grade and outcome of diagnosed DCIS (27) and decrease the costly, and potentially unnecessary, use of extensive surgery (eg, mastectomy or axillary lymph node excision)—the morbidity of which is not negligible (28,29). It would also reduce surgical scars, which might mimic lesions on subsequent MR images. In our pilot study, we found a significant negative correlation between ADC and DCIS grade. Furthermore, an ADC threshold was established to help identify low-grade DCIS lesions with very high specificity. In the future, the ADC could well become such a biomarker.

Contrast-enhanced MR imaging has been proposed in the grading of active tumors (8). However, it only reflects the tumor vascular bed and provides no information about tumor cellularity, which is important for determining tumor grade. The ADC has been shown to correlate with cellular density in breast cancer (17). We hypothesize that the increase in membrane density that accompanies active cell proliferation hinders water diffusion, resulting in a decrease in ADC (15). High-grade lesions with the highest cell proliferation rate would have the lowest ADCs, as in brain tumors (30,31). In breast tumors, however, this correlation between tumor cellularity and ADC is still controversial (17,32). Although it is considered that a DCIS tumor size of more than 2.5 cm has a higher risk of microinvasion or invasion (33), we did not find any correlation among overall lesion size, grade, and ADC, in accordance with a previous study (34).

Because of the multifocal nature of DCIS lesions, we based our first analysis on the use of all individual ROIs, an important step in depicting nonmass lesions, as several grades might be present at the same time. The statistical significance of the negative correlation found between tumor grade and ADC, as seen in invasive ductal carcinoma (17,19), suggests that the most malignant part of a tumor is associated with the ROI with the lowest ADC. Indeed, the concept of "minimum ADC" is central because, as shown in the spectrum of values seen in some of our patients, the values can vary. It is important to consider that although there are, of course, overlaps in the ADCs for the high-, intermediate-, and low-grade lesions in the patient population, it is apparently possible to establish a minimum ADC threshold of potential clinical importance with which to identify low-grade lesions.

The use of ROIs is much more robust and less sensitive to noise than is the use of voxel minimum ADC values that have sometimes been used (31,35). Approximately 4%–23% of biopsied DCIS lesions will eventually prove to be invasive breast cancer at final pathologic examination (36,37). Although the sensitivity of open excisional biopsy reaches almost 100%, it is not applied to all DCIS cases because of its invasiveness. One may argue that diffusion-weighted imaging does not have the resolution to depict invasiveness at a microscopic level compared with biopsy, but biopsy sampling is necessarily sparse and the possibility of scrutinizing the whole lesion with diffusion-weighted imaging, especially when different grades might coexist, may outbalance this limitation.

Most diffusion-weighted imaging studies of the breast have been performed at 1.5 T, with a wide range of *b* values (34,38,39), but ADC accuracy improves with *b* values of more than 850 sec/mm^2 at 3.0 T (40). Our choice of *b* values as high as 1000 sec/mm^2 was motivated by the low ADCs found in high-grade lesions, ADCs that are close to those in the brain. With large *b* values, lesions with low ADC appear with a much better contrast. This is especially useful in high-density breasts, where MR imaging appears to be better than mammography (41), and the prevalence of DCIS seems to be slightly higher for young women with high-density breasts (42).

A limitation of our study is the small population size; our minimum ADC threshold value might not be representative of that of a larger population, including patients with lesions other than DCIS. Because the ADC is also reduced in other breast malignancies (17,19), our minimum ADC concept could probably be extended to non-DCIS lesions pending further investigation with a larger patient cohort. Identification of lesions on diffusion-weighted images may not always be easy. Artifacts such as susceptibility, chemical shift, or distortion, for which diffusion-weighted echo-planar imaging is very sensitive, could impair ADC measurements (43). T2 shine-through and blackout effects, hemorrhage, necrosis, cystic lesions, or mucous protein components may cause changes in signal intensity on diffusion-weighted images. It is important to emphasize the need for high-quality diffusion-weighted images and fat suppression to achieve reliable quantitative diffusion MR images. Fat exhibits very low ADCs and may mimic high-grade lesions. Conversely, efficient fat suppression may also interfere with ADC measurements when fatty and tumor tissues overlap, possibly decreasing the signal intensity level substantially. It is always a good practice to check the overall signal intensity level before assessing borderline ADCs.

In summary, we found a negative correlation between ADC and DCIS grade. In addition, we determined an ADC threshold (1.3×10^{-3} mm^2/sec) that can help identify low-grade DCIS lesions with high specificity. Although further prospective assessment in a larger patient cohort is needed, the results of our study suggest that ADCs obtained with quantitative diffusion-weighted MR imaging may play a role as a highly specific biomarker for low-grade DCIS. Once the specificity of this approach is documented with further research, it might be possible to use conservative, minimally invasive approaches in patients with low-grade DCIS, which would decrease the economic and social burden associated with breast cancer (44). Diffusion-weighted imaging could also potentially help decrease the distress of women in whom low-risk DCIS has been diagnosed because they would be offered lighter treatment options than those treated for invasive breast cancer (45).

Acknowledgments: The authors thank Akitoshi Takamine, RT, Kiyoshi Kosaka, RT, and Teruaki Nishida, RT, of Kitano Hospital, Osaka, Japan, for their excellent technical assistance and kind support.

Disclosures of Potential Conflicts of Interest: **M.I.** No potential conflicts of interest to disclose. **D.L.B.** No potential conflicts of interest to disclose. **R.O.** No potential conflicts of interest to disclose. **T.O.** No potential conflicts of interest to disclose. **K.F.** No potential conflicts of interest to disclose. **S.K.** No potential conflicts of interest to disclose. **S.T.** No potential conflicts of interest to disclose. **M.F.** No potential conflicts of interest to disclose. **H.S.** No potential conflicts of interest to disclose. **K.T.** No potential conflicts of interest to disclose.

References

1. Ernster VL, Ballard-Barbash R, Barlow WE, et al. Detection of ductal carcinoma in situ in women undergoing screening mammography. J Natl Cancer Inst 2002;94(20):1546–1554.
2. Erbas B, Provenzano E, Armes J, Gertig D. The natural history of ductal carcinoma in situ of the breast: a review. Breast Cancer Res Treat 2006;97(2):135–144.
3. Sanders ME, Schuyler PA, Dupont WD, Page DL. The natural history of low-grade ductal carcinoma in situ of the breast in women treated by biopsy only revealed over 30 years of long-term follow-up. Cancer 2005;103(12):2481–2484.
4. Boecker W. Preneoplasia of the breast: a new conceptual approach to proliferative breast disease. Munich, Germany: Saunders Elsevier, 2006; 428.
5. Dinkel HP, Gassel AM, Tschammler A. Is the appearance of microcalcifications on mammography useful in predicting histological grade of malignancy in ductal cancer in situ? Br J Radiol 2000;73(873):938–944.
6. Kuhl C. The current status of breast MR imaging. I. Choice of technique, image interpretation, diagnostic accuracy, and transfer to clinical practice. Radiology 2007;244(2):356–378.
7. Berg WA, Gutierrez L, NessAiver MS, et al. Diagnostic accuracy of mammography, clinical examination, US, and MR imaging in preoperative assessment of breast cancer. Radiology 2004;233(3):830–849.
8. Neubauer H, Li M, Kuehne-Heid R, Schneider A, Kaiser WA. High grade and non-high grade ductal carcinoma in situ on dynamic MR mammography: characteristic findings for signal increase and morphological pattern of enhancement. Br J Radiol 2003;76(901):3–12.
9. Kuhl CK, Schrading S, Bieling HB, et al. MRI for diagnosis of pure ductal carcinoma in situ: a prospective observational study. Lancet 2007;370(9586):485–492.
10. Le Bihan D, Breton E, Lallemand D, Grenier P, Cabanis E, Laval-Jeantet M. MR imaging of intravoxel incoherent motions: application to diffusion and perfusion in neurologic disorders. Radiology 1986;161(2):401–407.
11. Le Bihan D. Molecular diffusion, tissue microdynamics and microstructure. NMR Biomed 1995;8(7-8):375–386.
12. Takahara T, Imai Y, Yamashita T, Yasuda S, Nasu S, Van Cauteren M. Diffusion-weighted whole body imaging with background body signal suppression (DWIBS): technical improvement using free breathing, STIR and high resolution 3D display. Radiat Med 2004;22(4):275–282.
13. Tamai K, Koyama T, Saga T, et al. The utility of diffusion-weighted MR imaging for differentiating uterine sarcomas from benign leiomyomas. Eur Radiol 2008;18(4):723–730.
14. Tamai K, Koyama T, Saga T, et al. Diffusion-weighted MR imaging of uterine endometrial cancer. J Magn Reson Imaging 2007;26(3):682–687.
15. Le Bihan D. The "wet mind": water and functional neuroimaging. Phys Med Biol 2007;52(7):R57–R90.
16. Kuroki-Suzuki S, Kuroki Y, Nasu K, Nawano S, Moriyama N, Okazaki M. Detecting breast cancer with non-contrast MR imaging: combining diffusion-weighted and STIR imaging. Magn Reson Med Sci 2007;6(1):21–27.
17. Guo Y, Cai YQ, Cai ZL, et al. Differentiation of clinically benign and malignant breast lesions using diffusion-weighted imaging. J Magn Reson Imaging 2002;16(2):172–178.
18. Woodhams R, Matsunaga K, Iwabuchi K, et al. Diffusion-weighted imaging of malignant breast tumors: the usefulness of apparent diffusion coefficient (ADC) value and ADC map for the detection of malignant breast tumors and evaluation of cancer extension. J Comput Assist Tomogr 2005;29(5):644–649.
19. Woodhams R, Matsunaga K, Kan S, et al. ADC mapping of benign and malignant breast tumors. Magn Reson Med Sci 2005;4(1):35–42.
20. Partridge SC, Demartini WB, Kurland BF, Eby PR, White SW, Lehman CD. Differential diagnosis of mammographically and clinically occult breast lesions on diffusion-weighted MRI. J Magn Reson Imaging 2010;31(3):562–570.

21. Silverstein M, Lagios M, Craig P, et al. The Van Nuys prognostic index for ductal carcinoma in situ. Breast J 1996;2(1):38–40.
22. Silverstein MJ, Lagios MD, Craig PH, et al. A prognostic index for ductal carcinoma in situ of the breast. Cancer 1996;77(11): 2267–2274.
23. Bianchi S, Vezzosi V. Microinvasive carcinoma of the breast. Pathol Oncol Res 2008; 14(2):105–111.
24. Jansen SA, Newstead GM, Abe H, Shimauchi A, Schmidt RA, Karczmar GS. Pure ductal carcinoma in situ: kinetic and morphologic MR characteristics compared with mammographic appearance and nuclear grade. Radiology 2007;245(3):684–691.
25. Tavassoli FA, Devilee P, eds. World Health Organization classification of tumours: pathology and genetics of tumours of the breast and female genital organs. Lyon, France: IARC Press, 2003.
26. SAS Institute. SAS/STAT user's guide, version 9.2. Cary, NC: SAS Institute, 2009.
27. Allegra CJ, Aberle DR, Ganschow P, et al. NIH state-of-the-science conference statement: diagnosis and management of ductal carcinoma in situ (DCIS). NIH Consens State Sci Statements 2009;26(2):1–27.
28. Silverstein MJ, Rosser RJ, Gierson ED, et al. Axillary lymph node dissection for intraductal breast carcinoma—is it indicated? Cancer 1987;59(10):1819–1824.
29. Baxter NN, Virnig BA, Durham SB, Tuttle TM. Trends in the treatment of ductal carcinoma in situ of the breast. J Natl Cancer Inst 2004; 96(6):443–448.
30. Kitis O, Altay H, Calli C, Yunten N, Akalin T, Yurtseven T. Minimum apparent diffusion coefficients in the evaluation of brain tumors. Eur J Radiol 2005;55(3):393–400.
31. Sugahara T, Korogi Y, Kochi M, et al. Usefulness of diffusion-weighted MRI with echo-planar technique in the evaluation of cellularity in gliomas. J Magn Reson Imaging 1999;9(1):53–60.
32. Yoshikawa MI, Ohsumi S, Sugata S, et al. Relation between cancer cellularity and apparent diffusion coefficient values using diffusion-weighted magnetic resonance imaging in breast cancer. Radiat Med 2008;26(4):222–226.
33. Maffuz A, Barroso-Bravo S, Nájera I, Zarco G, Alvarado-Cabrero I, Rodríguez-Cuevas SA. Tumor size as predictor of microinvasion, invasion, and axillary metastasis in ductal carcinoma in situ. J Exp Clin Cancer Res 2006;25(2):223–227.
34. Partridge SC, Mullins CD, Kurland BF, et al. Apparent diffusion coefficient values for discriminating benign and malignant breast MRI lesions: effects of lesion type and size. AJR Am J Roentgenol 2010;194(6):1664–1673.
35. Doskaliyev A, Yamasaki F, Ohtaki M, et al. Lymphomas and glioblastomas: differences in the apparent diffusion coefficient evaluated with high *b*-value diffusion-weighted magnetic resonance imaging at 3T. Eur J Radiol 2010. doi:10.1016/j.ejrad.2010.11.005. Published December 1, 2010.
36. Vlastos G, Verkooijen HM. Minimally invasive approaches for diagnosis and treatment of early-stage breast cancer. Oncologist 2007; 12(1):1–10.
37. Kettritz U. Modern concepts of ductal carcinoma in situ (DCIS) and its diagnosis through percutaneous biopsy. Eur Radiol 2008;18(2): 343–350.
38. Yabuuchi H, Matsuo Y, Okafuji T, et al. Enhanced mass on contrast-enhanced breast MR imaging: lesion characterization using combination of dynamic contrast-enhanced and diffusion-weighted MR images. J Magn Reson Imaging 2008;28(5):1157–1165.
39. Woodhams R, Kakita S, Hata H, et al. Identification of residual breast carcinoma following neoadjuvant chemotherapy: diffusion-weighted imaging—comparison with contrast-enhanced MR imaging and pathologic findings. Radiology 2010;254(2):357–366.
40. Bogner W, Gruber S, Pinker K, et al. Diffusion-weighted MR for differentiation of breast lesions at 3.0 T: how does selection of diffusion protocols affect diagnosis? Radiology 2009;253(2):341–351.
41. Kriege M, Brekelmans CT, Boetes C, et al. Efficacy of MRI and mammography for breast cancer screening in women with a familial or genetic predisposition. N Engl J Med 2004;351(5):427–437.
42. Gill JK, Maskarinec G, Pagano I, Kolonel LN. The association of mammographic density with ductal carcinoma in situ of the breast: the Multiethnic Cohort. Breast Cancer Res 2006;8(3):R30.
43. Park MJ, Cha ES, Kang BJ, Ihn YK, Baik JH. The role of diffusion-weighted imaging and the apparent diffusion coefficient (ADC) values for breast tumors. Korean J Radiol 2007; 8(5):390–396.
44. Pediconi F, Padula S, Dominelli V, et al. Role of breast MR imaging for predicting malignancy of histologically borderline lesions diagnosed at core needle biopsy: prospective evaluation. Radiology 2010;257(3):653–661.
45. Kennedy F, Harcourt D, Rumsey N, White P. The psychosocial impact of ductal carcinoma in situ (DCIS): a longitudinal prospective study. Breast 2010;19(5):382–387.

Breast Cancer
DOI 10.1007/s12282-011-0269-2

CASE REPORT

A case of metaplastic breast cancer that showed a good response to platinum-based preoperative chemotherapy

Haruko Takuwa · Takayuki Ueno · Hiroshi Ishiguro · Yoshiki Mikami · Shotaro Kanao · Masahiro Takada · Tomoharu Sugie · Masakazu Toi

Received: 11 January 2011 / Accepted: 4 April 2011

Abstract Patients with metaplastic breast cancer (MBC) exhibit reduced response to chemotherapy and have poor prognosis. We investigated a case of MBC that showed a positive response to preoperative chemotherapy, resulting in near pathological complete response (pCR). A 59-year-old woman complained of a lump in her right breast. Magnetic resonance imaging (MRI) showed the presence of a solid mass that was 24 mm in diameter. The pathological diagnosis was MBC with cartilaginous differentiation. The clinical stage was T2N0M0, stage IIA according to the International Union against Cancer (UICC) criteria. To observe the response to chemotherapy, we gave her preoperative chemotherapy. The patient was monitored closely, since we realized that failure of chemotherapy carries a risk of tumor progression. Evaluation was carried out using ultrasound, MRI, fluorodeoxyglucose (FDG) positron emission tomography (PET), and a Ki-67 labeling index after the first cycle of chemotherapy, and ultrasound after each additional cycle. FDG-PET showed a positive response after the first cycle of chemotherapy. The patient underwent 4 cycles of docetaxel (75 mg/m^2) and cisplatin (75 mg/m^2) followed by 4 cycles of cyclophosphamide (500 mg/m^2), doxorubicin (50 mg/m^2), and cisplatin (50 mg/m^2). Ultrasound showed decreases in tumor size after each cycle of chemotherapy. After chemotherapy, MRI showed nearly complete regression of the tumor. Partial mastectomy was performed. Pathological examination showed few cancer cells remaining, indicating near pCR. We report a case of MBC that responded well to platinum-based preoperative chemotherapy. We propose that preoperative chemotherapy may be an option for treatment of MBC in conjunction with careful monitoring.

Keywords Metaplastic breast cancer · Preoperative chemotherapy · FDG-PET · Ki67 labeling index · Monitoring

H. Takuwa · T. Ueno (✉) · M. Takada · T. Sugie · M. Toi
Department of Breast Surgery, Graduate School of Medicine, Kyoto University Hospital, 54 Shogoin kawara-cho, Sakyo-ku, Kyoto 606-8507, Japan
e-mail: takayuki@kuhp.kyoto-u.ac.jp

H. Ishiguro
Department of Chemotherapeutic Section for Outpatients, Graduate School of Medicine, Kyoto University Hospital, 54 Shogoin kawara-cho, Sakyo-ku, Kyoto 606-8507, Japan

Y. Mikami
Department of Pathology, Graduate School of Medicine, Kyoto University Hospital, 54 Shogoin kawara-cho, Sakyo-ku, Kyoto 606-8507, Japan

S. Kanao
Department of Radiology, Graduate School of Medicine, Kyoto University Hospital, 54 Shogoin kawara-cho, Sakyo-ku, Kyoto 606-8507, Japan

Introduction

The incidence of metaplastic breast cancer (MBC) is less than 1% of all breast cancers. Although MBC is reported to have a low rate of lymph node involvement [1, 2], the 5-year overall survival rate is 39–71%, in comparison with the 70–90% survival rate of breast cancer patients [1–8].

In most cases, immunohistochemical studies show estrogen receptor (ER)-negative, progesterone receptor (PgR)-negative, and HER2-negative (i.e., so-called triple-negative) phenotype. Using immunohistochemistry, Reis-Filho et al. [9, 10] reported that MBCs have a basal-like phenotype, regardless of the type of metaplastic element.

Published online: 28 April 2011

Triple-negative breast cancer is reported to show a 11–45% pathological complete response (pCR) rate following preoperative chemotherapy with anthracyclines and taxanes [11–13]. However, it is reported that MBC exhibits a poor response to chemotherapy [3]. There is a report showing that the pCR rate following preoperative chemotherapy for MBC is 10% [4]. In addition, the standard regimen for MBC is not well established [1, 3, 5, 7].

In this report, we describe the case of a patient with MBC who received preoperative chemotherapy with intensive monitoring and showed good response to a combination of platinum, anthracycline, and taxane, resulting in near pCR.

Case report

A 59-year-old woman presented with an irregularly shaped palpable mass (lump) in the right breast. MRI showed a polygonal solid mass with indistinct margins. The clinical stage was classified as T2N0M0, stage IIA (UICC criteria).

Mammotome biopsy revealed that the tumor was MBC with cartilaginous differentiation (Fig. 1) It was ER negative, PgR negative, HER2 negative, epidermal growth factor receptor (EGFR) positive, and cytokeratin (CK)5/6-negative, classified as a basal-like phenotype according to the report by Nielsen et al. [3, 10]. Ki-67 labeling index exceeded 80%, indicating a high tumor proliferating index.

MBC is usually resistant to chemotherapy, and standard chemotherapy regimens for its treatment have not been established. Even with systemic chemotherapy, the prognosis of MBC remains poor [1, 4, 6]. Some reports show that overall survival from MBC improves following aggressive multidisciplinary care, including chemotherapy [5, 7]. In addition, it has been reported that breast cancers with higher Ki67 index show greater sensitivity to chemotherapy. Thus, we considered that chemotherapy would improve the patient's prognosis. As there was a possibility that chemotherapy might not be effective, it was of utmost importance that our patient be closely monitored. We planned preoperative chemotherapy because intensive monitoring of the response to the treatment could be performed. To evaluate tumor response, we used ultrasound, MRI, FDG-PET, and a Ki-67 labeling index, after the first cycle of chemotherapy.

Some clinical trials have suggested that cisplatin is one of the most promising treatments for basal-like phenotype [1, 4], and we considered cisplatin the first option. We chose to use an established combination of docetaxel (75 mg/m^2) and cisplatin (75 mg/m^2) [14, 15] as an initial regimen.

Figure 1 shows the change in monitoring markers over the course of treatment. There was a 10% decrease in the Ki-67 labeling index (from 80% to 70%) in the core needle biopsy specimen on day 3. Although MRI on day 13 did not show any significant reduction in tumor size, PET on day 16 showed that the standardized uptake value (SUV) had decreased from 12.7 to 3.9, suggesting that chemotherapy was effective. We decided to continue chemotherapy. Tumor size measured by ultrasound decreased following the second cycle of chemotherapy.

As the treatment showed efficacy, we decided to continue the regimen. She did not experience serious adverse events, and the major toxicity she experienced was grade 1 nausea and grade 1 nail discoloration. Following 4 cycles of docetaxel and cisplatin, we chose a combination of cyclophosphamide (500 mg/m^2), doxorubicin (50 mg/m^2), and cisplatin (50 mg/m^2), an established regimen for endometrioid adenocarcinoma, since several reports show that anthracycline can also be effective against MBC [5, 7]. Ultrasound showed decreases in tumor size after each cycle of chemotherapy. The adverse events she had during this regimen included grade 1 nausea, grade 1 fatigue, and grade 1 peripheral sensory neuropathy.

After chemotherapy, MRI did not detect any obvious remaining mass (Fig. 1). PET showed a decrease in FDG uptake to almost normal levels in the tumor. The patient underwent partial resection of the right breast. The specimen showed few remaining cancer cells (Fig. 1). The therapeutic effect was determined to be grade 2b [16]. The patient has no recurrence 2 years and 6 months after the initiation of chemotherapy.

Discussion

We describe a case of MBC that showed good response to preoperative chemotherapy. In general, MBC shows poor response to chemotherapy, and surgical management is the first option. MBC is known to relapse frequently with distant metastasis [1, 3, 5, 7]. Some reports have shown that systemic chemotherapy might improve prognosis. Thus, we considered chemotherapy a necessary addition to surgical resection. We planned preoperative chemotherapy with careful monitoring to avoid rapid tumor growth in case the regimen was ineffective. Schwart-Dose et al. [17] and Rousseau et al. [18] showed that the pathological response of breast cancer to preoperative chemotherapy could be predicted accurately by FDG-PET, after the first or second cycle of chemotherapy. PET on day 16 of the first cycle showed a considerable decrease in SUV, suggesting that the treatment was effective. Based on this result, we decided to continue chemotherapy.

This case had triple-negative phenotype, for which there is no targeting therapy available so far. As the tumor had a basal-like phenotype with a high Ki-67 index, we thought

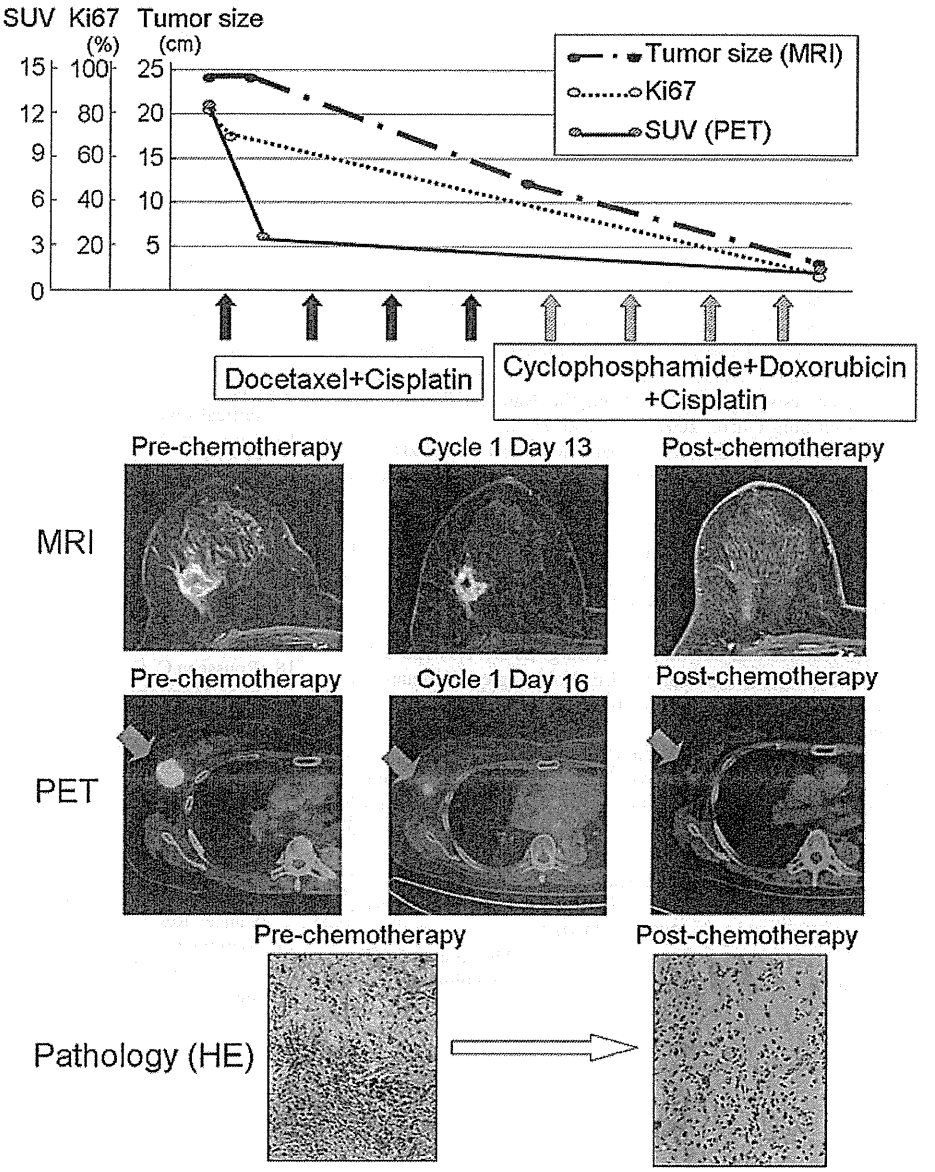

Fig. 1 Changes in tumor size, Ki67 labeling index, and standardized uptake value (SUV) during chemotherapy. FDG-PET showed a substantial decrease of SUV on day 16 of the first cycle of chemotherapy, although MRI did not show a significant decrease in tumor size. After completion of chemotherapy, PET showed almost normal levels of SUV in the tumor and MRI showed a considerable decrease in tumor size. Pathological examination revealed few remaining cancer cells after chemotherapy, indicating grade 2b therapeutic effect

that a regimen containing platinum, targeting poorly differentiated cancer cells and suggested to be a promising agent for basal-like breast cancer, might be effective [14, 15]. Since the standard chemotherapy regimen for operable breast cancer is a taxane- and anthracycline-based regimen, we decided to combine cisplatin with taxane or anthracycline. We chose a regimen of 4 cycles of docetaxel (75 mg/m^2) and cisplatin (75 mg/m^2) followed by 4 cycles of cyclophosphamide (500 mg/m^2), doxorubicin (50 mg/m^2), and cisplatin (50 mg/m^2).

Preoperative chemotherapy was so effective that it achieved near pCR. In general, pCR is a surrogate marker for recurrence-free survival. Near pCR refers to near-total disappearance of invasive tumor with only focal tumor residues in the removed breast tissue [19]. It has been reported that near pCR indicates longer disease-free survival in patients with remnant cancer cells following preoperative chemotherapy [20, 21]. In this case near pCR of the tumor was achieved, suggesting improved survival. The patient has no recurrence 2.5 years after the initiation of chemotherapy. However, as the aforementioned reports did not include MBC cases, the impact of near pCR in MBC patients is uncertain. Thus, careful follow-up is required for this case.

We describe a case of MBC for which preoperative chemotherapy containing platinum, taxane, and anthracycline was effective. PET was useful to monitor efficacy of the treatment. We propose that, in conjunction with careful

monitoring, preoperative chemotherapy may be an option for treating patients with MBC.

Acknowledgments We thank Dr. Tomomi Nishimura for taking photos of pathology and Ms. Akiko Shiomi and Ms. Kikuko Fujita for their technical assistance with the manuscript.

References

1. Chao TC, Wang CS, Chen SC, Chen MF. Metaplastic carcinomas of the breast. J Surg Oncol. 1999;71(4):220–5.
2. Pezzi CM, Patel-Parekh L, Cole K, Franko J, Klimberg VS, Bland K. Characteristics and treatment of metaplastic breast cancer: analysis of 892 cases from the National Cancer Data Base. Ann Surg Oncol. 2007;14(1):166–73.
3. Al Sayed AD, El Weshi AN, Tulbah AM, Rahal MM, Ezzat AA. Metaplastic carcinoma of the breast clinical presentation, treatment results and prognostic factors. Acta Oncol. 2006;45(2):188–95.
4. Hennessy BT, Giordano S, Broglio K, Duan Z, Trent J, Buchholz TA, et al. Biphasic metaplastic sarcomatoid carcinoma of the breast. Ann Oncol. 2006;17(4):605–13.
5. Gibson GR, Qian D, Ku JK, Lai LL. Metaplastic breast cancer: clinical features and outcomes. Am Surg. 2005;71(9):725–30.
6. Rayson D, Adjei AA, Suman VJ, LE Wold, Ingle JN. Metaplastic breast cancer: prognosis and response to systemic therapy. Ann Oncol. 1999;10(4):413–9.
7. Beatty JD, Atwood M, Tickman R, Reiner M. Metaplastic breast cancer: clinical significance. Am J Surg. 2006;191(5):657–64.
8. Dave G, Cosmatos H, Do T, Lodin K, Varshney D. Metaplastic carcinoma of the breast: a retrospective review. Int J Radiat Oncol Biol Phys. 2006;64(3):771–5.
9. Reis-Filho JS, Milanezi F, Steele D, Savage K, Simpson PT, Nesland JM, et al. Metaplastic breast carcinomas are basal-like tumours. Histopathology. 2006;49(1):10–21.
10. Cheang MC, Voduc D, Bajdik C, Leung S, Mc Kinney S, Chia SK, et al. Basal-like breast cancer defined by five biomarkers has superior prognostic value than triple-negative phenotype. Clin Cancer Res. 2008;14(5):1368–76.
11. Rouzier R, Perou CM, Symmans WF, Ibrahim N, Cristofanilli M, Anderson K, et al. Breast cancer molecular subtypes respond differently to preoperative chemotherapy. Clin Cancer Res. 2005;11(16):5678–85.
12. Heys SD, Sarkar T, Hutcheon AW. Primary docetaxel chemotherapy in patients with breast cancer: impact on response and survival. Breast Cancer Res Treat. 2005;90(2):169–85.
13. Smith IC, Heys SD, Hutcheon AW, Miller ID, Payne S, Gilbert FJ, et al. Neoadjuvant chemotherapy in breast cancer: significantly enhanced response with docetaxel. J Clin Oncol. 2002;20(6):1456–66.
14. Downs-Kelly E, Nayeemuddin KM, Albarracin C, Wu Y, Hunt KK, Gilcrease MZ. Matrix-producing carcinoma of the breast: an aggressive subtype of metaplastic carcinoma. Am J Surg Pathol. 2009;33(4):534–41.
15. Rakha EA, Reis-Filho JS, Ellis IO. Basal-like breast cancer: a critical review. J Clin Oncol. 2008;26(15):2568–81.
16. Kurosumi M, Akashi-Tanaka S, Akiyama F, Komoike Y, Mukai H, Nakamura S, et al. Histopathological criteria for assessment of therapeutic response in breast cancer (2007 version). Breast Cancer. 2008;15(1):5–7.
17. Schwarz-Dose J, Untch M, Tiling R, Sassen S, Mahner S, Kahlert S, et al. Monitoring primary systemic therapy of large and locally advanced breast cancer by using sequential positron emission tomography imaging with [18F]fluorodeoxyglucose. J Clin Oncol. 2009;27(4):535–41.
18. Rousseau C, Devillers A, Sagan C, Ferrer L, Bridji B, Campion L, et al. Monitoring of early response to neoadjuvant chemotherapy in stage II and III breast cancer by [18F]fluorodeoxyglucose positron emission tomography. J Clin Oncol. 2006;24(34):5366–72.
19. Kuroi K, Toi M, Tsuda H, Kurosumi M, Akiyama F. Issues in the assessment of the pathologic effect of primary systemic therapy for breast cancer. Breast Cancer. 2006;13(1):38–48.
20. Toi M, Nakamura S, Kuroi K, Iwata H, Ohno S, Masuda N, et al. Phase II study of preoperative sequential FEC and docetaxel predicts of pathological response and disease free survival. Breast Cancer Res Treat. 2008;110(3):531–9.
21. Symmans WF, Peintinger F, Hatzis C, Rajan R, Kuerer H, Valero V, et al. Measurement of residual breast cancer burden to predict survival after neoadjuvant chemotherapy. J Clin Oncol. 2007;25(28):4414–22.

Proc. of SPIE, Vol. 7899, pp. 78992J-1—78992-J-7, 2010.

Characterization of photoacoustic tomography system with dual illumination

Kazuhiko Fukutani*[a], Yasuhiro Someda[a], Masakazu Taku[a], Yasufumi Asao[a,c], Shuichi Kobayashi[a], Takayuki Yagi[a], Makoto Yamakawa[b], Tsuyoshi Shiina[c], Tomoharu Sugie[c], and Masakazu Toi[c]
[a]Medical Imaging Project, Canon Inc., 3-30-2 Shimomaruko, Ohta-ku, Tokyo, Japan 146-8501;
[b]Advanced Biomedical Engineering Research Unit, Kyoto University, Kyoto, Japan;
[c]Graduate School of Medicine, Kyoto University, 54 Shogoin-Kawaharacho, Sakyo-ku, Kyoto, Japan 606-8507

ABSTRACT

In this study, we characterized a newly developed imaging system, "dual illumination mode photoacoustic tomography (PAT) system". The PAT system can simultaneously or separately illuminate biological tissues from a forward and backward direction toward an array transducer. The shape of the custom-made transducer is rectangular, which allows direct illumination of tissue surfaces in front of the array transducer through a holding plate from the backward direction. The transducer frequency was designed at 1 MHz by considering the trade-off relationship between ultrasound attenuation and image resolution. A Ti:Sa laser optically pumped with a Q-switched Nd:YAG laser, having a tunable wavelength of 700 to 900 nm, was chosen for deep light penetration in tissues. The laser light was sufficiently expanded and homogenized to keep the level of laser-pulse fluence on the sample surface under the ANSI safety limit. System performance was tested with phantoms. The results of our study showed that the system visualized all the absorbers embedded in a 50-mm-thick tissue-mimicking phantom with a lateral resolution of 2~3 mm.

Keywords: photoacoustic tomography, deep tissue imaging, dual illumination

1. INTRODUCTION

Breast cancer is the most common malignant tumor among women and has one of the highest incidences of any cancer in developed countries [1]. Each year, more than 190,000 American women are diagnosed with breast cancer, and almost 41,000 will lose their lives to the disease [1]. Early detection is the largest contributing factor to decreasing breast cancer mortality. Thus, a reliable modality for breast cancer diagnosis is needed. The generally used modalities, such as ultrasound imaging (US), x-ray mammography (MMG) and magnetic resonance imaging (MRI) have some drawbacks. MMG can image abnormal areas of density, mass, and calcification that may indicate the presence of cancer; however, it uses ionizing radiation, strongly compresses the breast and its performance is lower for dense breasts because the cancer is hidden by dense tissue. These are disadvantages for younger women. US can visualize the shape of cysts that characterize potential abnormalities seen on MMG images, which helps to determine if the abnormality is solid (such as a benign fibroadenoma or solid cancer) or fluid-filled (such as a benign cyst). However, US is dependent on the operator's skill. The results of an US diagnosis reflect the ability of the technologist or radiologist to properly manage the equipment. MRI is effective in imaging a breast cancer and provides functional imaging; however, expensive equipment and contrast agents, which are contraindicated for some patients, are required for MRI.

Vascularization is one of the most important characteristics of cancers, but in the abovementioned modalities it is difficult to image vascularization even when using contrast agents. Recently, photoacoustic imaging (PAI) has proved useful as a promising imaging modality that can visualize biological tissues with high contrast and high spatial resolution at relatively low cost [2]. In the photoacoustic (PA) effect, the tissue is irradiated using nanosecond laser pulses, which leads to thermoelastic expansion generated upon heating of optically absorbing structures. Pressure waves produced by the themoelastic expansion are detected by an acoustic transducer placed at various positions outside the sample, and the images are reconstructed from the detected signals. Finally, PAI provides a distribution of optical absorption contrast,

* fukutani.kazuhiko@canon.co.jp; phone +81 3 3758 2111; fax +81 3 3757 3096

Photons Plus Ultrasound: Imaging and Sensing 2011, edited by Alexander A. Oraevsky, Lihong V. Wang,
Proc. of SPIE Vol. 7899, 78992J · © 2011 SPIE · CCC code: 1605-7422/11/$18 · doi: 10.1117/12.873690

which is related to physiological properties such as hemoglobin concentration and tissue oxygen consumption. Therefore, it is expected that vascularization can be easily imaged by PAI instead of using MRI assisted by contrast agent. So far, several groups have reported the results of a pilot study on breast cancer diagnosis using PAI [3,4].

Meanwhile, deep tissue imaging in PAI remains difficult due to strong light scattering in biological tissues. For breast cancer diagnosis without hard compression, an imaging depth of over 50 mm is desired. However, the strong light scattering in biological tissues exponentially attenuates the optical fluence, and consequently, it is too difficult to detect PA signals emitted from deep tissues. There are several approaches for deep tissue imaging. One is to increase the sensitivity of the acoustic detector [5,6]. Song *et al.* developed a reflection-mode PA imaging system using a focused ultrasonic transducer with a large active element and successfully imaged absorbers embedded 38 mm deep in chicken breast tissue [5]. Ma *et al.* used a 2D capacitive micromachined ultrasonic transducer array and imaged absorbers embedded as deep as 50 mm inside a tissue-mimicking phantom [6]. Another approach is to use contrast agents [7,8]. Ku *et al.* used indocyanine green (ICG) dye and imaged ICG-filled tubes at depths greater than 50 mm in chicken breast tissue [7]. Kim *et al.* used methylene blue (MB) and imaged MB-filled tubes at a depth of 52 mm in biological tissues [8].

In this study, we developed a new photoacoustic tomography (PAT) system with dual illumination mode, which simultaneously illuminates tissues from a forward and backward direction toward an array transducer. In contrast to previous studies [5-8], the dual illumination mode PAT system makes deep tissue imaging possible in terms of light penetration without hard compression of tissues.

2. SYSTEM DESIGN AND METHOD

2.1 Dual illumination mode PAT system

To achieve deep tissue imaging, we designed a new system, the "dual illumination mode PAT system," as shown schematically in Fig.1 (a). The system simultaneously illuminates a sample from the forward and backward direction toward an array transducer to increase optical fluence in the region-of-interest (ROI) of the sample. In addition, the sample is gently compressed by two transparent holding plates. The gentle compression of the sample also contributes light penetration into the deep tissue. A transducer is contacted with a side of the holding plate through the oil. Here, x and y represent the horizontal and vertical direction of the transducer position, respectively, and the z-axis is the depth direction.

Details of the system setup are as follows. Two sets of a Ti:Sa laser (LT-2211, LOTIS TII) optically pumped with a Q-switched Nd:YAG laser (LS-2137, LOTIS TII) are used as the excitation source to provide 15-ns laser pulses with a 10-Hz pulse repetition rate. One is used for backward illumination, and the other for forward illumination. To maximize the optical fluence of the ROI in the samples, the laser light illuminates the sample surface from the forward and backward direction at the same time, which is called the "dual illumination mode" in our system. On the other hand, the system also has an "alternately illumination mode" that illuminates the sample from a forward and backward direction separately. In the alternately illumination mode, the optical properties of the background medium can be estimated by minimizing the difference between the ratio of the initial pressure distribution obtained from the illumination modes and the calculated light fluence distribution [9]. In the backward illumination, the laser light is divided into two beams by a beam splitter and the two lights illuminate to the sample surface from the side of the transducer through the holding plate. The incident angle of laser light is determined by Monte Carlo simulation to maximize the optical fluence in the ROI. Although the Ti:Sa laser can be tuned from 700 to 900 nm, we chose a wavelength of 797 nm to achieve deep penetration of light in this study. These light configurations make deep tissue imaging possible in terms of light penetration. The maximum output power of the Ti:Sa laser is ~80 mJ. The maximum permissible exposure (MPE) of laser fluence incident on the tissue is limited to ~31 mJ/cm^2 in accordance with the ANSI safety standard at the wavelength of 797 nm [10]. Thus, laser lights from the backward and forward direction are sufficiently expanded by a concave lens and finally homogenized by a diffuser to satisfy the MPE limit. In this study, the maximum incident laser energy density from backward and forward illumination of the sample surface is ~3 and ~9 mJ/cm^2, respectively. These values are approximately 1/10 and 1/3, respectively, of the ANSI safety limit.

A 2D 345-element (15(x) × 23(y)) transducer with element size of 2×2 mm^2 is designed for our system. The shape of the transducer is rectangular, which allows direct illumination of tissue surfaces in front of the array transducer through a

10-mm-thick holding plate. The transducer frequency is designed at 1 MHz with a bandwidth greater than 70% in order to optimize the trade-off relationship between receiving deep PA signals with minimal ultrasonic attenuation and obtaining appropriate resolution for breast cancer diagnosis. The array was custom fabricated by Vermon S.A. (France) using piezocomposite technology for high sensitivity and signal-to-noise ratio. The array detects PA signals at one position, which corresponds to a detection area of 30×46 mm^2. The custom made front-end electronics and data acquisition system was used to obtain PA signals for image reconstruction. The front-end electronics consist of 345-channel receivers. Scanning starts by triggering the response of a photodiode from the laser light at the instant when the optical pulse illuminates the sample. In this study, we used a fixed amplifier gain of 40 dB, 20 MHz sampling rate, and sampling data of 1280 points. The received PA signals are amplified, filtered, and digitized in the front-end electronics, and the digitized PA signals are transferred to the PC for further signal processing and image reconstruction.

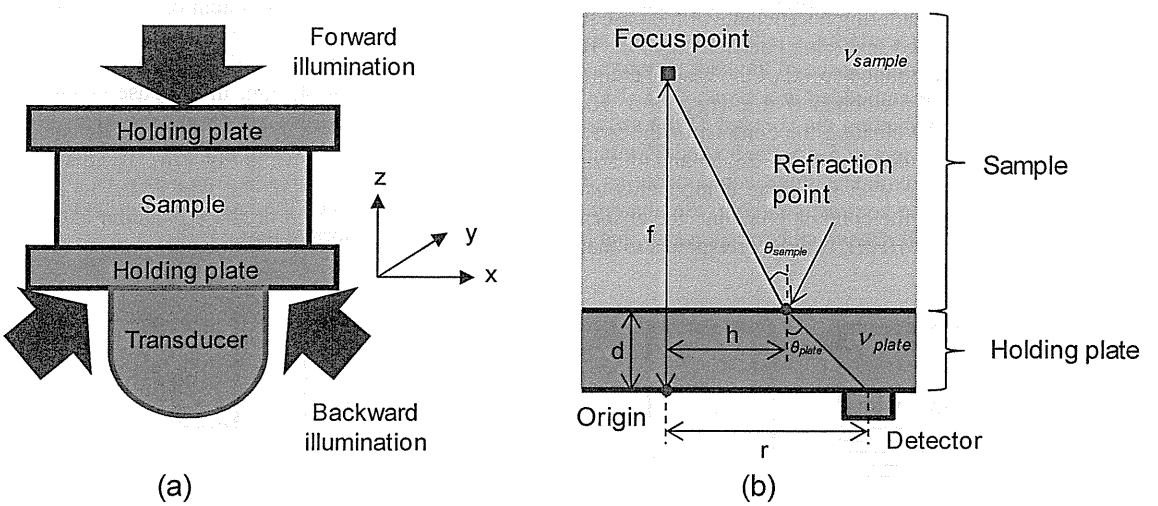

Figure 1. (a) Schematic diagram of the dual illumination mode PAT system. (b) Refraction effect due to holding plate.

2.2 Image reconstruction

Since PA signals are detected by the 2D array transducer through the 10-mm-thick holding plate, we modified a universal backprojection algorithm [11] to take account the effect of the plate. The sound speed of the holding plate (v_{plate}) is 2200 m/s, which is much faster than that of typical tissue (v_{sample}), 1500 m/s. Therefore, refraction occurs at the interface between the tissue sample and holding plate. Figure 1(b) shows a schematic diagram of the refraction effect due to the holding plate. This refraction causes blurred images if an algorithm assuming constant sound speed is used. From Snell's law, the equation including a refraction point, h, is given by

$$\frac{v_{sample}}{v_{plate}} = \frac{\sin\theta_{sample}}{\sin\theta_{plate}} = \frac{h/\sqrt{h^2+(f-d)^2}}{(r-h)/\sqrt{d^2+(r-h)^2}}. \qquad (1)$$

where f, r, and d are the distance between the origin and focus point, the distance between origin and detector, and thickness of the holding plate, respectively. By solving Eq. (1), we can obtain h. If h is given, the propagation distance of the pressure wave between the detector and the focus point (R) is written as follows:

$$R = \sqrt{h^2+(f-d)^2} + \frac{v_{sample}}{v_{plate}} \cdot \sqrt{d^2+(r-h)^2}. \qquad (2)$$

We introduced the modified distance R into the backprojection algorithm assuming a constant sound speed of the sample for refraction correction. Furthermore, the reconstructed PA images were corrected by the predicted light distribution, calculated by the finite-element method, based on a diffusion equation. Reconstruction was implemented on a graphic processing unit (GPU) to reduce the reconstruction speed. The typical size of reconstructed volume is 30(x) × 46(y) × 50(z) mm^3, which is the same volume as the size of the array transducer multiplied by the thickness of the phantom. Since the voxel pitch is set to 0.25 mm in each direction, the number of voxels corresponds to 120×184×200. The reconstruction time for the voxels takes less than 2 s on a PC with a 240 core GPU.

2.3 Phantoms

System performance was tested by using tissue-mimicking phantoms with embedded absorbers. The base of the tissue-mimicking phantom with a size of 70(x) × 120(y) × 50(z) mm^3 was made with urethane gel and curing agent. The absorption and reduced scattering coefficients of the base phantom were adjusted by adding titanium oxide and india ink. The absorption and reduced scattering coefficients of the base phantom were 0.0096 and 1.00 mm^{-1} at the wavelength of 797 nm, respectively. The sound speed of the base phantom was 1366 m/s. For evaluating lateral resolution of the system, 0.3-mm rubber wires were embedded at a depth of 5, 10, 15, 20, 25, 30, 35, 40 and 45 mm in the base phantom, as shown in Fig. 2(a). For evaluating the contrast of the system, 2-mm tube absorbers with absorption coefficient of 0.03 mm^{-1} were embedded at a depth of 5, 15, 25, 35 and 45 mm in the base phantom, as shown in Fig. 2(b). The inserted tube absorbers were also made with the same components as that of the base phantom, but ink was added to adjust the absorption coefficient. In the contrast phantom, the absorption coefficient ratio between the base phantom and the tube absorber is approximately 10 dB, which corresponds to that between cancerous and normal tissue [12].

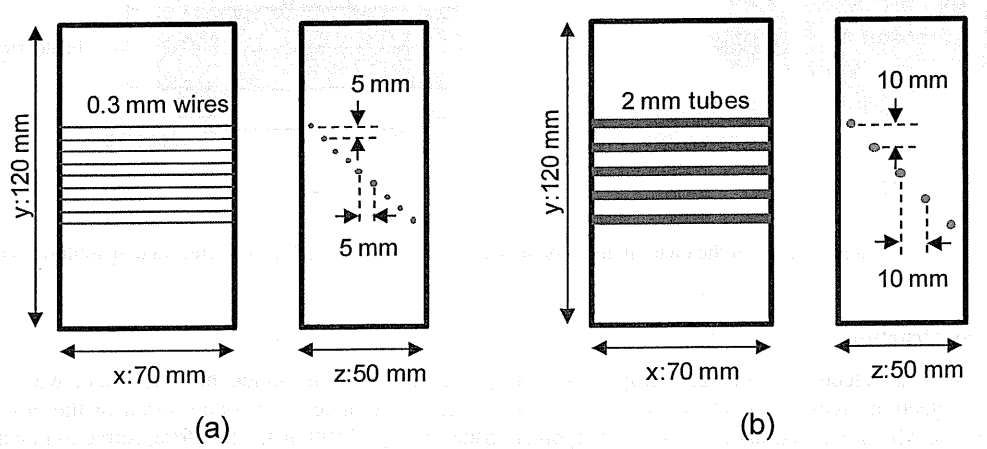

Figure 2. Structure of tissue-mimicking phantoms for (a) resolution and (b) contrast evaluation.

3. RESULTS AND DISCUSSIONS

3.1 Refraction correction

To confirm the effect of refraction correction on the reconstructed images, two images with and without correction are compared. Figure 3 shows slice images on the x-y plane of reconstructed volumes with and without refraction correction. In this case, the 0.3-mm wire absorbers embedded at a depth of 25 mm in the phantom were imaged for resolution evaluation. We can see that the blurring is significantly reduced by compensating the refraction effect. The lateral resolution of the image with refraction correction is almost the same as that obtained from the PAT system without the holding plate.